



## Experiment on obtaining maps of solar magnetic fields with the spectrograph of the Solar Tower Telescope 2 at CrAO

A.A. Plotnikov, A.S. Kutsenko, D.G. Semyonov, G.A. Sunitsa

Crimean Astrophysical Observatory, Nauchny 298409  
e-mail: [plotnikov.andrey.alex@yandex.ru](mailto:plotnikov.andrey.alex@yandex.ru)

Received 17 April 2024

### ABSTRACT

The paper describes the experiment on the solar magnetic field measurements with the spectrograph of the Solar Tower Telescope 2 (STT-2). Using a charge-coupled device (CCD), the data on solar spectra in two polarization states were collected by two consecutive scans of the solar surface. The polarization of the light beam was decoded by a quarter-wave plate and a linear polarizer. The recorded spectra were processed to derive I and V Stokes profiles, which were further inverted under the Milne–Eddington atmosphere model. The method provides spatial maps of the longitudinal magnetic field component and magnetic field strength. A shortcoming of the method is the necessity to carry out two consecutive scans of the solar surface in different polarization states rather than simultaneous capturing of orthogonal polarization states using a beam splitter unit. However, the approach yielded acceptable results and showed satisfactory agreement with the data provided by the Helioseismic and Magnetic Imager on board the Solar Dynamics Observatory. We found that the polarization crosstalk of the telescope may produce false polarization signals and requires special attention.

**Key words:** magnetic field, spectropolarimetry, Sun

### 1 Introduction

Physical conditions of the atmosphere affect the absorption of passing light by atoms and, as a consequence, form a unique dependence of radiation intensity on wavelength (the so-called spectral line profile) in each case. Obviously, the analysis of the shape of such a profile allows one to obtain information about the physical parameters in the corresponding region of the atmosphere.

Measurements of the magnetic field vector in the solar atmosphere are of considerable interest in solar physics. One of the observable manifestations of the magnetic field is the Zeeman effect, which is a splitting of magnetically sensitive spectral lines in the presence of a magnetic field. The magnitude of the splitting turns out to be proportional to the magnitude of the magnetic field modulus, and the analysis of the degree of polarization of the split components also allows one to obtain information about the orientation of the magnetic field vector.

Systematic measurements of solar magnetic fields have been carried out for quite a long time. Visual observations began back in 1908 at the Mount Wilson Observatory (Hale et al., 1919). In this case, the observer visually estimates the splitting between spectral components, which is subsequently recalculated into the magnetic field magnitude. It turns out difficult to obtain a clear spatial distribution of the magnitude, so in practice only the maximum magnetic fields in

individual sunspots are measured. Such measurements have been carried out since 1957 and to this day with the STT-2 telescope at CrAO (Severny, Stepanov, 1956).

The use of photomultiplier tubes (PMTs) and electro-optical polarization modulators made it possible to automate the measurement process. The magnetograph scheme was proposed in Babcock (1953), and it was subsequently implemented at CrAO (Nikulin, Severny, 1958). The setting of the PMT slit on one of the wings of the magnetically active line and consecutive passing of one or the other circular polarization through the analyzer leads to the fact that the amplitude of the PMT output signal becomes proportional to the longitudinal magnetic field component. The use of the second PMT in the symmetrical position on the other wing of the line makes it possible to increase the signal-to-noise ratio (and, consequently, the measurement accuracy). For accurate positioning of the PMT slits relative to the line center, a plane-parallel plate is used to compensate for the Doppler shift of the line. The measured line-of-sight velocity is assumed to be proportional to the plate inclination. Introducing the third PMT allows one to simultaneously obtain maps with the spatial distribution of brightness and with the measurement of the longitudinal magnetic field component (hereinafter  $B_z$ ).

The mentioned methods are the attempts of limited analyzing the shape of spectral line profiles within the technical capabilities of that time. A robust analysis requires obtaining

the so-called data cube that is the distribution of intensity both in two spatial and in spectral coordinates. Recording such a volume of data using a PMT would take an unacceptably long time, and in practice such measurements became possible only with the advent of two-dimensional electronic detectors (CCD and CMOS arrays).

The difficulties are not limited to the data recording process. A separate difficulty is the process of extracting the values of the parameters of interest. For their full calculation, it is required to solve the so-called inverse problem (or inversion). Its essence is as follows: using a model for the assumed set of parameters, a theoretical spectral profile is constructed, which is compared with the actually observed one. The set of parameters at which the theoretical profile differs least from the observed one is taken as the measured values.

In the described approach, there are three variable factors: the model for constructing the theoretical profile, the function of the difference between two profiles (“loss function”), and the method for selecting the optimal data set. An increase in spatial and spectral resolution leads to a multiple increase in computational complexity. The inversion of the spectral profile in each pixel is a separate and independent task. Even for a map of  $100 \times 100$  pixels (which is a rather small size by the standards of modern instruments), it is required to solve  $10^4$  separate tasks. The development of technology made it possible to process such volumes of data only 20–30 years ago, but even today these tasks still require significant computing resources.

As mentioned above, solar magnetic fields are currently measured only by the visual method at the STT-2 telescope of CrAO RAS. This approach is very interesting in the context of the presence of a long series of observations, but it provides a very sparse set of data by modern standards. Meanwhile, the existing equipment allows one to significantly expand the amount of information obtained from observations without invoking a serious restructuring of the existing telescope. In this paper, we describe an experiment on recording spectra taken with STT-2 in different polarization states using a CCD array. We also present the results of their subsequent processing by inverting the profiles within the framework of the Milne–Eddington atmosphere model (ME inversion) to obtain spatial maps of the magnetic field and other parameters of the solar atmosphere.

## 2 Equipment and methods

The observations were carried out with the STT-2 telescope of CrAO RAS. The optical scheme of the telescope, described in detail in [Stepanian et al. \(2014\)](#), includes a primary mirror with a diameter of 200 mm and a focal length of 8 m. In combination with a Cassegrain mirror with a diameter of 180 mm, a solar image of 140 mm is constructed at the spectrograph slit. The spectrograph consists of a collimating mirror with a focal length of 7.5 m, a diffraction grating with a groove density of  $600 \text{ mm}^{-1}$ , and camera mirrors.

The spectrograph scheme was changed for the experiment. In the dispersion plane, an MTO-11 lens with a focal length of 1000 mm was installed as a camera. The detector was an Atik Titan CCD receiver with a Sony ICX424 sensor ( $658 \times 492$  pixels) with a pixel size of  $7.4 \times 7.4 \text{ }\mu\text{m}$ .

The Fe I 6302.5 Å spectral line with an effective Lande factor of 2.5 was used for observations. The spectrum was recorded in the fourth spectral order of the grating. To isolate the spectral region, an OST-12 broadband filter was used.

In this work, we decided to limit ourselves to recording only circular polarization (I and V components of the Stokes vector). Firstly, linear polarization is affected by large measurement noise and requires a significantly higher calibration accuracy of instrumental polarization. Secondly, as shown earlier in [Plotnikov, Kutsenko \(2018\)](#), circular polarization is sufficient to measure not only the longitudinal component but also the magnitude of the magnetic field vector modulus.

To obtain the I and V components of the Stokes vector, it is required to record the spectrum in two polarizations: left circular (I – V) and right circular (I + V). Ideally, images in both polarizations should be recorded simultaneously, which is achieved, for example, using a polarizing beam splitter (Wollaston prism, Glan prism, etc.). Consecutive recording when passing a beam through the analyzer of one or the other polarization can give a less accurate result: due to atmospheric fluctuations, the corresponding positions of the slit on the solar disk do not exactly coincide. However, in this work, we decided to evaluate the applicability of this approach in general. To isolate circular polarization, a quarter-wave plate and a linear polarizer were installed in front of the spectrograph slit.

To obtain a data cube, the image of the solar disk is shifted across the spectrograph slit, and the spectrum is recorded sequentially in each position (the spectrograph slit “scans” the image of the solar disk). Thus, the following sequence was performed: at the beginning, the analyzer was set to transmit left circular polarization (for this, the fast axis of the plate  $\lambda/4$  was oriented at an angle of  $45^\circ$  relative to the axis of the linear polarizer) and the area of interest was scanned; after this the transmitted polarization was changed into right circular by rotating the polarizer axis by 90 degrees and the same area was re-scanned. The electronic scheme providing the scanning is described in [Semyonov et al. \(2021\)](#).

After such a procedure, we obtain two data cubes in the first approximation corresponding to the polarization states (I – V) and (I + V). By addition or subtraction, they can be converted into cubes of Stokes parameters I and V. Due to the inaccuracy of the clock drive, the spatial coordinates in the two cubes may not coincide. To eliminate errors caused by such a shift, it is necessary to align the corresponding images using some contrasting object, for example, a sunspot. For this, before performing the addition and subtraction operations, the cubes were cropped so that the center of mass of the sunspot image had the same spatial coordinates.

Figure 1 shows an example of the obtained Stokes parameters I and V for one of the positions of the spectrograph slit. The slit is pointed to small spots, so one can observe a decrease in intensity in the umbra and penumbra and an increase in the amplitude of the V parameter accompanying the magnetic fields. In the left part of the spectrum, the telluric line 6302.8 Å is also visible. The presence of a constant circular polarization is noticeable on the V component (marked by the black arrow), which looks physically unjustified. Apparently, the reason for the appearance of the V signal may be small vibrations of the spectrograph elements due to which the position of the spectrum on the detector may shift during consecutive scans. When calculating the difference in inten-

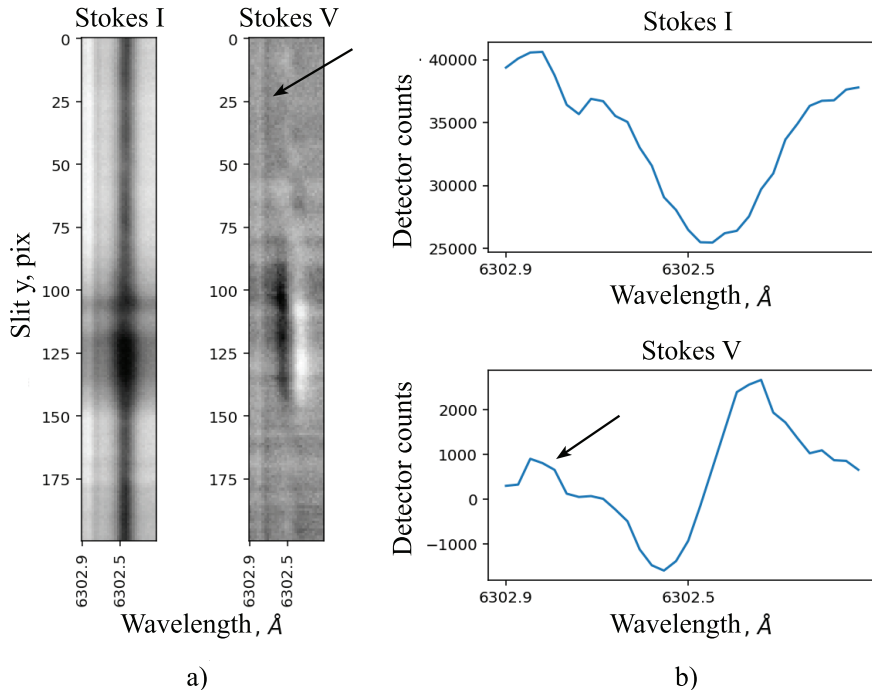


**Fig. 1.** Example of Stokes parameters I and V obtained at STT-2. (a) – a slice of the data cubes in one of the scanning positions. The spectrograph slit is pointed to small spots. (b) – a slice of the image in panel (a) at the level  $y = 125$ . The black arrow marks the parasitic intensity V in the atmospheric line.

sities in two polarizations, this may lead to the appearance of a parasitic signal. Thus, when using consecutive scans, special attention should be paid to the alignment of the obtained images in spatial and spectral coordinates.

As mentioned in Introduction, for a robust analysis of spectral profiles, it is required to solve the inverse problem regarding their formation in the solar atmosphere.

The Milne–Eddington model was used as an atmosphere model. It consists of the following assumptions:

1. Local thermodynamic equilibrium.
2. The source function increases linearly with optical depth.
3. The remaining parameters of the atmosphere do not change along the optical depth.

For the photosphere where the lines are formed in a fairly narrow range in height, such assumptions can be considered justified.

The main advantage of this model is the presence of an analytical solution for the radiative transfer equation (the Unno–Rachkovsky solution (Unno, 1956; Rachkovsky, 1962)). This fact significantly increases the rate of constructing model profiles and, as a consequence, the rate of solving the inverse problem.

As a function for comparing the observed and theoretical profiles (“loss function”), the sum of the squares of the point-by-point differences (MSE) was used. The Levenberg–Marquardt method was used to search for the optimal set of parameters. Such a combination is widely used to solve inverse problems (see Table 1 in del Toro Iniesta, Ruiz Cobo, 2016).

The following parameter values were used as the initial approximation:

1. Magnetic field strength: 1000 G.
2. The angle between the magnetic field vector and the line of sight (inclination): 45 deg.
3. Doppler line width: 20 mÅ.
4. Line strength: 10.
5. Source function at zero optical depth: 0.5 of the continuum intensity.
6. Source function gradient: 0.5 of the continuum intensity per unit optical depth.
7. Doppler shift (line-of-sight velocity): 0 km/s.

The azimuth of the magnetic field (the direction of the vector projection onto the plane perpendicular to the line of sight) does not affect the shape of the I and V profiles and therefore cannot be calculated with the obtained data set. The line damping (Lorentzian broadening) weakly changes the final line profile and, in order to simplify the problem, may not be fitted (Borrero et al., 2011). A value of 0.5 of the Doppler width of the profile was adopted for it.

The processing program was written in the Python programming language using the Astropy (Astropy Collaboration et al., 2022), Sunpy (The SunPy Community et al., 2020), Numpy (Harris et al., 2020), and Scipy (Virtanen et al., 2020) libraries. The images were generated using the Matplotlib library (Hunter, 2007).

### 3 Results

The observations were carried out on July 18, 2023, around 16:00. The NOAA AR 13372, located at coordinates N23W13, was studied.

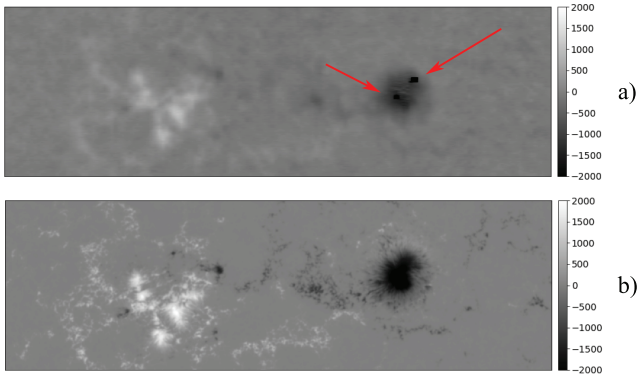


**Fig. 2.** Magnetograms of the longitudinal magnetic field component for NOAA AR 13372 obtained from STT-2 observations (a) and SDO/HMI (b). Red arrows mark pixels with outliers.

Figure 2a shows the obtained  $B_z$  map. Despite the low spatial resolution of the image, the main details of the active region can be seen, as well as the supergranulation network. For comparison, Fig. 2b shows the corresponding  $B_z$  map obtained by the Solar Dynamics Observatory/Helioseismic Magnetic Imager (SDO/HMI; Pesnell et al., 2012; Scherrer et al., 2012).

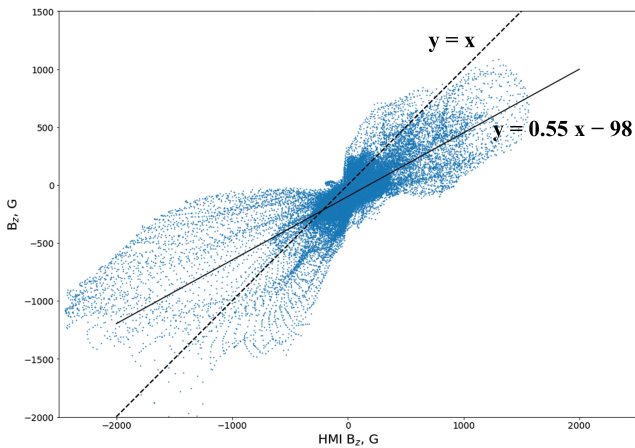


**Fig. 3.** Scatter plot for the values of the longitudinal magnetic field component obtained in this work and from the SDO/HMI data. Gaussian smoothing with  $\sigma = 3''$  is applied to the SDO/HMI data.

Figure 3 shows a scatter plot between the  $B_z$  values obtained in this work and from the SDO/HMI data. To match the spatial resolutions, Gaussian smoothing with  $\sigma = 3''$  was applied to the SDO/HMI data. A good correlation between the data is noticeable ( $R = 0.68$ ). Moreover, due to the imperfect spatial alignment of the images obtained by the two instruments, the calculated correlation between the maps may be somewhat lower than the real value.

It can be seen that the values obtained in this work are underestimated by about 1.8 times compared to similar SDO/HMI data (the slope of the linear approximation is 0.55). In the sunspot umbra, the ME inversion gives an inclination of the field to the line of sight of about 60–70 degrees,

which does not correspond to sunspot models and other observations. Both of these facts together suggest that the Stokes V parameter in the STT-2 measurements is underestimated compared to the real values, for example, due to the effects of instrumental polarization. An insufficient amplitude of the V parameter leads, in turn, to underestimated values of  $B_z$ .

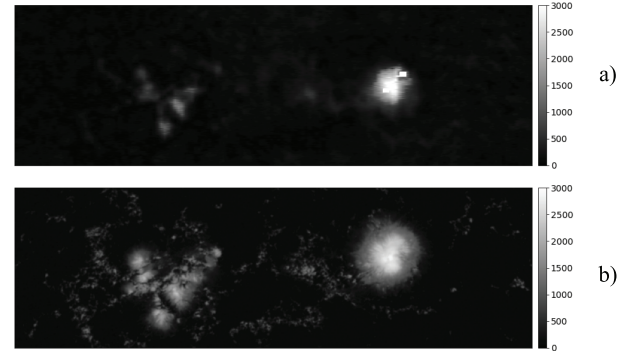


**Fig. 4.** Magnetograms of the magnetic field modulus for NOAA AR 13372 obtained from STT-2 observations (a) and SDO/HMI (b).

Figure 4 shows a comparison of maps for the modulus of the magnetic field vector. There is a coincidence of data for the zone of strong fields and the quiet Sun, but in the penumbra zone, the values differ even visually. Presumably, due to the underestimation of the Stokes V parameter in the inclined field of the penumbra, the ratio between the shifted  $\sigma$ - and unshifted  $\pi$ -components is distorted, which leads to an incorrect calculation of the field modulus. This problem is absent in the longitudinal field at the center of the sunspots where only  $\sigma$ -components are present.

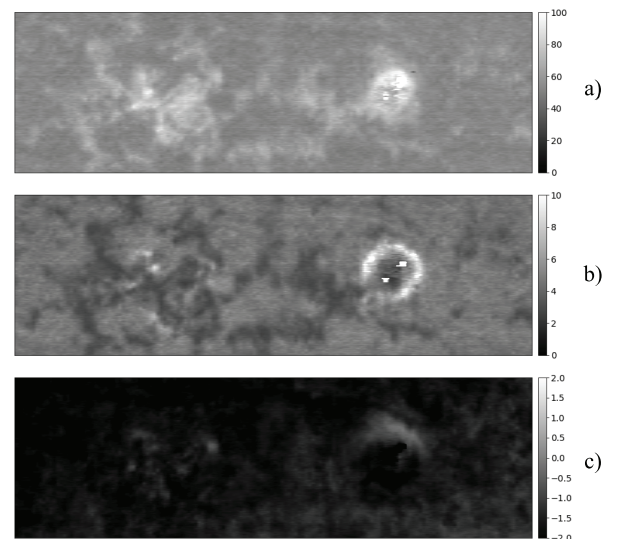


**Fig. 5.** Maps of the parameters obtained from STT-2 observations: Doppler width (a), line strength (b), line-of-sight velocity (c).

As mentioned above, the ME inversion allows one to obtain maps not only of the magnetic field vector but also of other parameters. Some of these maps (Doppler width, line strength, and line-of-sight velocity) are shown in Fig. 5.

In a number of pixels, outliers of parameters can be seen, and their position coincides on all maps (marked by red arrows in Fig. 2). This indicates inversion problems at these points, and apparently, a more careful selection of the initial approximation is required.

## 4 Conclusions

This work presents the results of recording data from the STT-2 spectrograph using a CCD array in various polarizations and their subsequent inversion in the approximation of the Milne–Eddington atmosphere. Despite the simplified polarimeter scheme (consecutive scanning in two polarization states instead of using a polarizing beam splitter), the results can be considered satisfactory. The maps of the longitudinal magnetic field component demonstrate good visual agreement and correlation with the data of the space instrument SDO/HMI.

Meanwhile, a statistical underestimation of  $B_z$  is noted. We tend to believe that this is due to the effects of instrumental polarization. Each mirror in the telescope system can contribute to the distortion of the polarization picture, and the mirrors of the coelostat system, in which reflections often occur at angles that differ greatly from the normal, require special attention (Beck et al., 2005).

The influence of scattered light can also be considered as an additional factor. An estimate of the scattering near the limb gives a value of about  $1 \div 2\%$  of the intensity at the center of the disk, which in the zone of sunspots (where the intensity drops by  $10 \div 20$  times compared to the quiet Sun zone) can make a significant contribution to the distortion of the degree of polarization.

Fixed initial approximations for the inverse problem turn out to be sufficient at most points, but in some cases lead to a physically inadequate solution. Special attention is required in the umbra zone where the radiation intensity is reduced and the signal-to-noise ratio drops significantly. For a more thorough selection of the initial parameters, simplified meth-

ods for estimating parameters or machine learning methods can be used.

The work was supported by the state assignment No. 122022400224-7.

## References

- Astropy Collaboration, Price-Whelan A.M., Lim P.L., et al., 2022. *Astrophys. J.*, vol. 935, no. 2, p. 167.
- Babcock H.W., 1953. *Astrophys. J.*, vol. 118, p. 387.
- Beck C., Schlichenmaier R., Collados M., Bellot Rubio L., Kentischer T., 2005. *Astron. Astrophys.*, vol. 443, no. 3, pp. 1047–1053.
- Borrero J.M., Tomczyk S., Kubo M., et al., 2011. *Solar Phys.*, vol. 273, no. 1, pp. 267–293.
- del Toro Iniesta J.C., Ruiz Cobo B., 2016. *Liv. Rev. Sol. Phys.*, vol. 13, no. 1, p. 4.
- Hale G.E., Ellerman F., Nicholson S.B., Joy A.H., 1919. *Astrophys. J.*, vol. 49, p. 153.
- Harris C.R., Millman K.J., van der Walt S.J., et al., 2020. *Nature*, vol. 585, no. 7825, pp. 357–362.
- Hunter J.D., 2007. *Comp. Sci. Eng.*, vol. 9, no. 3, pp. 90–95.
- Nikulin N., Severny A., 1958. *Izv. KrAO*, vol. 19, pp. 3–19.
- Pesnelli W.D., Thompson B.J., Chamberlin P.C., 2012. *Solar Phys.*, vol. 275, no. 1–2, pp. 3–15.
- Plotnikov A., Kutsenko A., 2018. *Izv. KrAO*, vol. 114, no. 2, pp. 87–96.
- Rachkovsky D., 1962. *Izv. KrAO*, vol. 28, pp. 259–270.
- Scherrer P.H., Schou J., Bush R.I., et al., 2012. *Solar Phys.*, vol. 275, no. 1–2, pp. 207–227.
- Semyonov D., Sunitsa G., Kutsenko A., 2021. *Izv. KrAO*, vol. 117, no. 1, pp. 15–21.
- Severny A., Stepanov V., 1956. *Izv. KrAO*, vol. 16, pp. 3–12.
- Stepanian N., Sunitsa G., Malashchuk V., 2014. *Izv. KrAO*, vol. 110, no. 1, pp. 107–122.
- The SunPy Community, Barnes W.T., Bobra M.G., et al., 2020. *Astrophys. J.*, vol. 890, p. 68.
- Unno W., 1956. *Publ. Astron. Soc. Japan*, vol. 8, p. 108.
- Virtanen P., Gommers R., Oliphant T.E., et al., 2020. *Nature Methods*, vol. 17, pp. 261–272.